Shear-Layer Effects on the Dynamics of a Counter-Rotating Vortex Pair

Thomas Hofbauer*and Thomas Gerz†
Institute of Atmospheric Physics, DLR Oberpfaffenhofen
Weßling, Germany

The influence of three-dimensional wind–shear layers (jets) on the transport and decay of a counter-rotating vortex pair is investigated by means of direct numerical simulation. A laminar case is considered where the jet width varies periodically along the vortex axis. Further, the impact of two turbulence levels in the jet upon the vortex pair is studied. The initially laminar vortex pair penetrates from above into the jet and towards the ground. When penetrating into the laminar jet the wake vortices experience a sinusoidal perturbation but do not link. Contrarily, mutually independent dissolution of each vortex is observed when the jet is turbulent. The upstream vortex with vorticity opposing the vorticity of the upper shear layer of the jet starts to erode when it touches the upper flank of the turbulent jet, whereas the downstream vortex remains unaffected until it interacts with the lower shear layer below the jet maximum. The vortex breakdown process and its spatial structure is discussed in detail.

Nomenclature

b	Vortex spacing, m
k, k_p	Wavenumber, peak wavenumber
p'	Dynamic pressure deviation, Nm^{-2}
r	Radial distance from vortex core, m
r_c	Radius of vortex core, m
Re_Γ	$= \Gamma/\nu$, Reynolds number
u_i	velocity vector, ms^{-1}
U_{cw}	Mean crosswind velocity, ms^{-1}
V_θ	Azimuthal velocity of single vortex, ms^{-1}
v_{rms}	Root-mean-square velocity, ms^{-1}
x, y, z	Spanwise, axial, and vertical direction in Cartesian coordinates, m
Γ	Vortex circulation, m^2s^{-1}
δ	Jet layer depth, m
ℓ	Turbulence integral length scale, m
λ_2	Vortex identification parameter, s^{-2}
ν	Kinematic viscosity, m^2s^{-1}
ω_y, ω_θ	Axial, azimuthal vorticity component, s^{-1}
ρ	Constant air density, $kg\,m^{-3}$

Introduction

As an unavoidable consequence of lift, aircraft generate pairs of counter-rotating trailing vortices which constitute a potential hazard to following aircraft. In order to assure flight safety, separation standards are set-in which prescribe the minimum separation distance between leader and follower aircraft during take-off, approach, and landing. Today, such standards are uniquely based on the maximum take-off weights of the aircraft pair. Experience and extensive studies,[?] however, emphasize that vortex transport and decay, and hence the hazard, strongly depend on the atmospheric conditions. From the encounter experience during the past 30 years, it became evident that the separation standards are rather conservative guesses in a variety of meteorological situations. At the same time, these standards limit the throughput capacity of some major airports. Driven by the increase of world's air traffic, this situation will become more severe in the near future. Therefore, attempts are underway which aim at optimizing the separation standards by taking into account the local meteorological condition.

In order to ensure flight safety, it has to be guaranteed that the wake vortices from the leading aircraft have either irreversibly left the flight corridor or decayed. A forecasting model capable of accurately predicting the vortex positions and strengths in a given and forecasted atmospheric environment along the flight path might therefore permit air-traffic controllers to ease some of the regulations without loss of safety. The essential key towards such a model is knowledge about the meteorological processes and their impact on the wake vortex behaviour.

The main atmospheric parameters that influence vortex lifetime and transport are ambient turbulence, crosswind, wind shear and thermal stratification. Crosswind may carry the vortices away from a security sector whereas turbulence and thermally unstable[?] and even stable stratification[?] enhance the decay of vortices. Crosswind shear, on the other hand, is a candidate that causes tilting of the vortex pair, accompanied by increased vortex separation.[?] Furthermore, vortices can impressively rebound on shear layers, whereupon the vortex with opposing vorticity to the vorticity of the shear layer tends to rebound

*PhD student, email: Thomas.Hofbauer@dlr.de
†Research Scientist, email: Thomas.Gerz@dlr.de

stronger.

Vortex aging and decay often manifests in different processes: The vortex linking and the subsequent formation of vortex rings — often referred to as large–scale or Crow instability[?] — presents one primary destruction mechanism for aircraft wakes. Short–wave or Widnall instability[?] may play a significant role when the distance between the vortex tubes diminishes.[?] Another mechanism is vortex breakdown which may be characterized as an abrupt change in structure of a vortex tube. Because of a sudden increase of the vortex core diameter, this phenomenon is often refered to as vortex–core bursting. Sarpkaya and Daly[?] investigated the effect of grid-generated (close to isotropic) turbulence in a towing tank on the lifespan of trailing vortices. They pointed out that the triggering mechanism which precedes the destruction of the vortices depends on the level of ambient turbulence: sinusoidal instability occurs at weak turbulence levels while strong turbulence results in vortex bursting. In moderate turbulence either sinusoidal instability or core bursting occurred. The sinusoidal instability did not result in linking but, on contrary, vortex separation often increased and the vortex pair rolled from a horizontal to an almost vertical position.

More recently, Risso *et al.*[?] and Gerz and Holzäpfel[?] investigated the wake vortex behaviour in homogeneous and anisotropic turbulence by means of direct numerical simulations (DNS) and large–eddy simulations (LES). They found that the effect of turbulence can be separated into two different mechanisms: the large scale turbulence causes antisymmetric deformations on the vortices, whereas small turbulent structures promote the diffusion of vorticity out of the vortex cores. Risso *et al.* postulated that azimuthal structures around the main vortices, which were formed by stretching environmental turbulent eddies in the vicinity of the vortices, are responsible for the vortex deformation which initiates the long wave (Crow) instability.

Purpose of this study is to demonstrate the prominent effect of ambient shear on the vortex behaviour. In particular, we consider a background "low-level" jet stream. Besides a laminar jet, we further investigate the impact of turbulent jets upon the vortex evolution. The observed breakdown of the vortices for the turbulent cases is discussed in detail.

Numerics, Initialization, and Cases

The numerical model used in this study solves the Navier-Stokes equations for an incompressible fluid, i.e.

$$\frac{\partial u_i}{\partial x_i} = 0 \tag{1}$$

$$\frac{\partial u_i}{\partial t} + \frac{\partial}{\partial x_j} u_i u_j = -\frac{1}{\rho}\frac{\partial p'}{\partial x_i} + \nu \frac{\partial}{\partial x_j}\frac{\partial}{\partial x_j} u_i. \tag{2}$$

Time advancement is performed by a prognostic step for advection and diffusion using the second-order Adams-Bashforth scheme followed by a diagnostic step which solves the Poisson equation for the dynamic pressure. On a Cartesian staggered grid, the spatial derivatives are approximated by explicit second-order central finite differences. The model exhibits the property of being nondissipative and weakly diffusive. A description of the model can be found in Schumann *et al.*[?].

The coordinate system is chosen such that the initially parallel vortex tubes are aligned along the $y-$axis (flight direction of aircraft); the jet stream blows spanwise in $x-$direction. Free-slip and rigid-lid boundary conditions are used for the bottom and the top of the computational domain. For the boundaries in spanwise direction, inflow (Dirichlet) and outflow (Neumann) conditions for the velocity components are applied and periodicity is assumed in axial direction.

Vortex Initialization

The wake vortex pair generated by aircraft is the result of the roll-up process of the vortex sheet which is shed by the lifting wing. As we are interested in the far-field characteristics we do not account for these near-field processes and start our simulation with already mature vortices. The simulations are initialized by the linear superposition of two counter-rotating Lamb-Oseen vortices with circulation $\Gamma_0 = \pm 250\, m^2/s$, initial core radius $r_c = 3m$, and separation $b_0 = 24\, m$, which roughly characterize a Boeing-727 wake.

The vortices are embedded in different background shear flows, as described below. In the following, quantities marked with an asterisk are normalized using Γ_0 and b_0 as reference scales. Hence, reference velocity is 10.42 m/s and reference time amounts to 2.3 s. The azimuthal velocity V_θ^* of a solitary Lamb-Oseen vortex is given as a function of radius r^* with respect to its center by

$$V_\theta^*(r^*) \;=\; \frac{1}{2\,\pi\, r^*}\left(1 - e^{-\beta (r^*/r_c^*)^2}\right) \tag{3}$$

where $\beta = 1.2564$ is a constant.

Setup of the Laminar Background Flow

We investigate the behaviour of a vortex pair subjected to a laminar low-level jet, whose crosswind profile $U_{cw}^*(y^*, z^*)$ is given by

$$U_{cw}^*(y^*, z^*) = U_{max}^*\left(1 + cos\left(\frac{\pi\,(z^* - z_0^*)}{\delta^*(y^*)}\right)\right) \tag{4}$$

with a sinusoidally varying thickness δ^* in axial direction y^* that follows

$$\delta^*(y^*) = \delta_{mean}^* - \delta_{var}^* \cdot cos(\,2\,\pi\, y^* /\, y_{max}^*) \tag{5}$$

with mean value $\delta_{mean}^* = 1.5$ and variation $\delta_{var}^* = 0.5$. The wavelength of the variation is equal to the domain

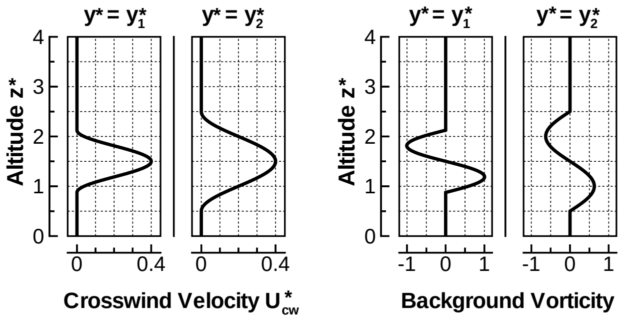

Fig. 1 Crosswind profiles and shear–layer vorticity for the extrema of the variation. The vortex pair is initiated at $z^* = 3$.

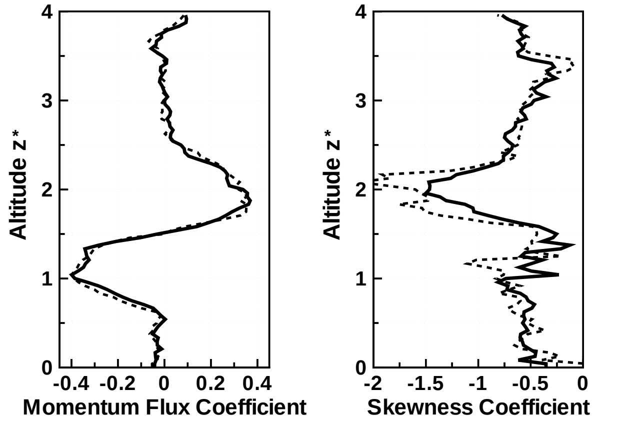

Fig. 2 Momentum flux coefficient and skewness coefficient for times $t^* = 0$ (solid) and $t^* = 3.04$ (dashed).

size in axial direction $y^*_{max} = 4$. The maximal jet velocity amounts to $U^*_{max} = 0.4$ and is situated at $z^*_0 = 1.5$ ("low–level jet"). For illustration, $U^*_{cw}(y^*_1, z^*)$ and $U^*_{cw}(y^*_2, z^*)$ are shown in Figure 1 where $y^*_1 = 0$ and $y^*_2 = y^*_{max}/2$ mark the axial positions of the maximum variation. The vortex pair has been initialized at $z^* = 3$.

Setup of the Turbulent Background Flow

To study the effect of a turbulent jet on a trailing vortex pair, a preparatory simulation is necessary in order to obtain appropriate initial conditions. Starting at $t^* = -5.64$, we allow the initially isotropic turbulence with a spectral energy-density slope of $exp(-k^2/k_p^2)$ to develop in the mean shear environment, eq. 4, without aircraft vortices. Figure 2 depicts the vertical profiles of the mean momentum flux coefficient C_u and the mean skewness coefficient S_u,

$$C_u(z^*) = \frac{\overline{u'^* \, w'^*}}{\sqrt{\overline{u'^{*2}} \; \overline{w'^{*2}}}}, \tag{6}$$

$$S_u(z^*) = -\frac{1}{3} \, \overline{\left(\frac{\partial u'^*}{\partial x^*}\right)^3} \cdot \left[\overline{\left(\frac{\partial u'^*}{\partial x^*}\right)^2} \right]^{-3/2}, \tag{7}$$

for two time levels; the bars denote horizontal averages. The profiles of C_u reveal that the flux of momentum from the mean jet to the turbulent flow is well established above and below the wind maximum. The negative values of $S_u(z^*)$ show that also the transfer of turbulent energy from large to small scales is fully developed.

The root-mean-square velocity fluctuations v_{rms} are chosen to be approximately 5 and 10% of the maximum mean jet velocity U^*_{max}. The most energetic eddies are as large as the half of the mean jet thickness. This corresponds to a turbulence integral scale of $\ell^* \approx 0.21$ and an eddy turn-over time of $\ell^*/v^*_{rms} \approx 5.4$. Hence, we observe that roughly after one turn-over time, the environmental flow has reached a statistically (quasi) stationary state. This serves now as initial condition for the main simulation where we linearily superimpose the flow field from the preparatory run at $t^* = 0$ with the flow field of the vortices, eq. 3. The result is plotted in Figure 4a below.

Cases

The characteristics of the cases presented here are summarized in Table 1. The domain dimensions are $(L^*_x, L^*_y, L^*_z) = (10.7, 4.0, 4.0)$.

Case	Resolution	Re_Γ	v^*_{rms}
L	$256 \times 64 \times 96$	4400	–
T0	$256 \times 64 \times 96$	4400	0.038
T1	$512 \times 128 \times 192$	4400	0.038
T2	$256 \times 64 \times 96$	4400	0.019

Table 1: Case characteristics; L laminar, T turbulent cases.

Case L denotes the laminar case. Case T0 which constitutes the reference case in this study has same mean properties as case L but its low-level jet is turbulent with intensity in terms of root-mean-square velocity v^*_{rms}. Case T1 serves as a run to check resolution requirements. In Case T2 the turbulence intensity is half as large as in Case T0.

Results

Laminar Low-Level Jet

Figure 3 depicts coherent flow structures of case L at two instants of time.[?] We use the vortex identification scheme developed by Jeong and Hussain[?], who proposed that the second eigenvalue λ_2 of $S_{ik}S_{ki} + \Omega_{ik}\Omega_{ki}$ (where S_{ik} and Ω_{ik} are the symmetric and anti-symmetric parts of the velocity gradient tensor $\partial u_i/\partial x_j$, respectively) is a suitable measure to represent coherent structures in turbulent flows. Figure 3 illustrates the atmospheric jet by two iso-surfaces of $\lambda^*_2 = -1$ for each shear layer. In this perspective view the inflow boundary, located at $x^* = 0$, is on the right. At the same time, location and structure of the primary vortices are shown as dark tubes by iso-surfaces of a second value $\lambda^*_2 = -53$. As expected, the variation of the jet–layer thickness δ initiates a variation

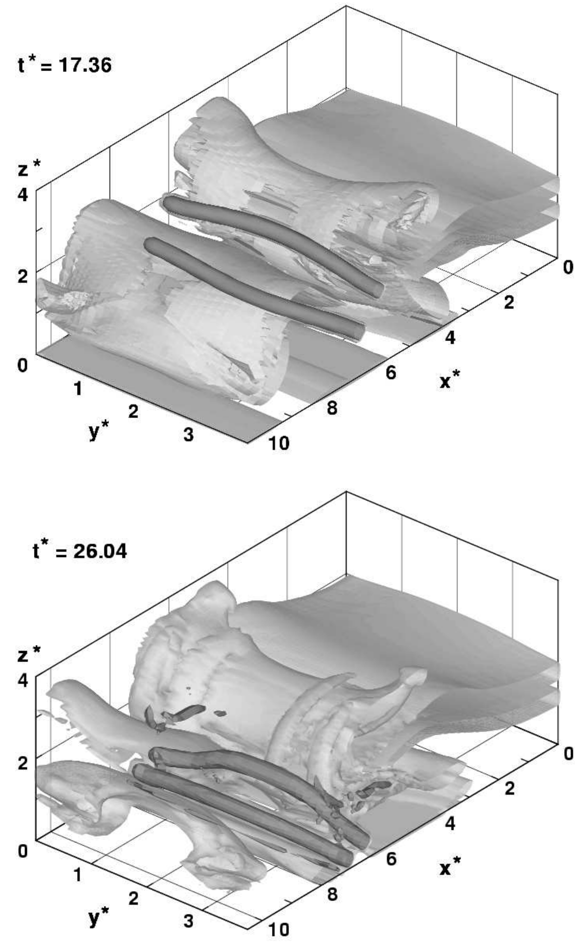

Fig. 3 Case L: Interaction of the vortex pair with laminar wind jet and ground. Isosurfaces of λ_2^*=-1 (for the jet) and -53 (for the aircraft vortex pair).

in vortex separation at the same wavelength which is evident at $t^* = 17.36$. As Crow[?] showed, such perturbations of the vortex separation grow exponentially in time, leading to a linking of the vortex pair and, eventually, to its rapid destruction. However, at the same time the vortices diverge as a result of their interaction with secondary vortices from the shear layer. This mitigates the growth rate of the instability mechanism. In our case the two vortices approach each other but they do not link because when interacting with the ground they separate again.

Turbulent Low-Level Jet

Now we repeat case L by considering a turbulent environment. The preparatory simulation to obtain appropriate initial conditions is described in the previous section. Figure 4 shows iso-surfaces in terms of λ_2^* for early times of case T0. At $t^* = 5.43$, the vortices have descended and already begun to interact with the turbulent jet flow. A small perturbation on the upwind vortex at $y^* \approx 1$ is apparent. At $t^* = 8.68$, this perturbation has amplified to a quickly growing instability that resembles a vortex core bursting event.

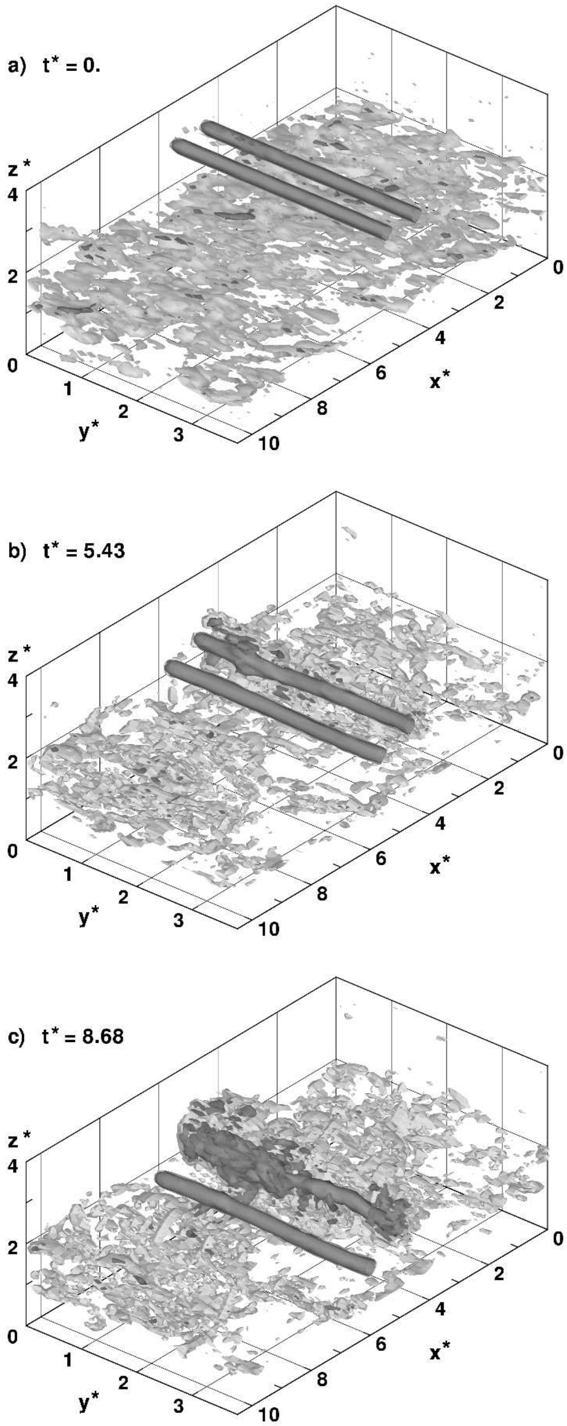

Fig. 4 Case T0: Onset of decay of upstream vortex. Parameters as in previous Figure.

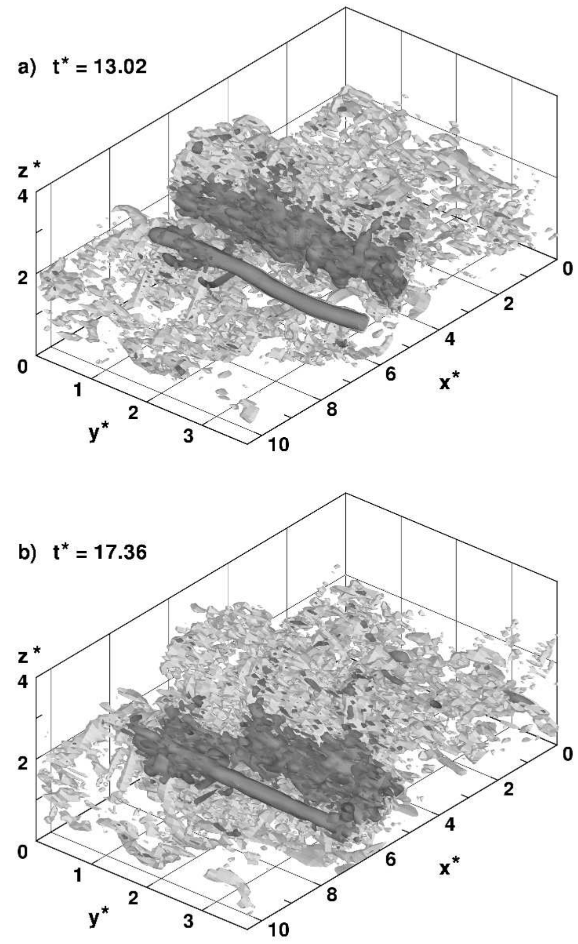

Fig. 5 Case T0: Final period of decay of upstream vortex, onset of decay of downstream vortex. Parameters as in previous Figure.

The perturbation seems to propagate along the vortex axis. For later times, see Figure 5, the downwind vortex experiences the same fate: The perturbation at the vortex tube becomes visible at $t^* = 13$ and also seems to travel along the vortex. At that time the upwind vortex appears to be fully eroded.

In case T1 with the same physics as case T0 but with double resolution in each direction the flow exhibits the same flow structures as in case T0. As to be expected, structures at small scales appear more clearly (not shown). Figure 6 compares the structures of the trailing vortices for cases T0 and T2 at one instant of time; both cases reveal intact downstream vortices whereas the upstream partners have both lost their contiguous structure at that time. It is remarkable that the upstream vortex is more bended and more diffuse when the turbulence intensity of the jet is lower (case T2).

Figure 7 provides quantitative information by comparing evolutions of circulations from the upwind and downwind vortices of the laminar and the turbulent cases. Γ has been obtained by integrating ω_y in circular areas with radii of $r = 3r_c$ and averaging over axial direction y. In case L the downstream vortex retains its initial circulation whereas its upstream partner levels off at about $0.94\Gamma_0$. The loss of 6% is due to the contribution of vorticity from the upper half of the jet in which the upper vortex penetrates. In all turbulent cases T0, T1, and T2, the circulations of the upstream vortices start to decay at about $t^* = 2$ and follow approximately the respective curve of case L until $t^* \approx 6$ when the circulations of all turbulent cases start to decay quickly. They obtain values of 0.35, 0.45, and

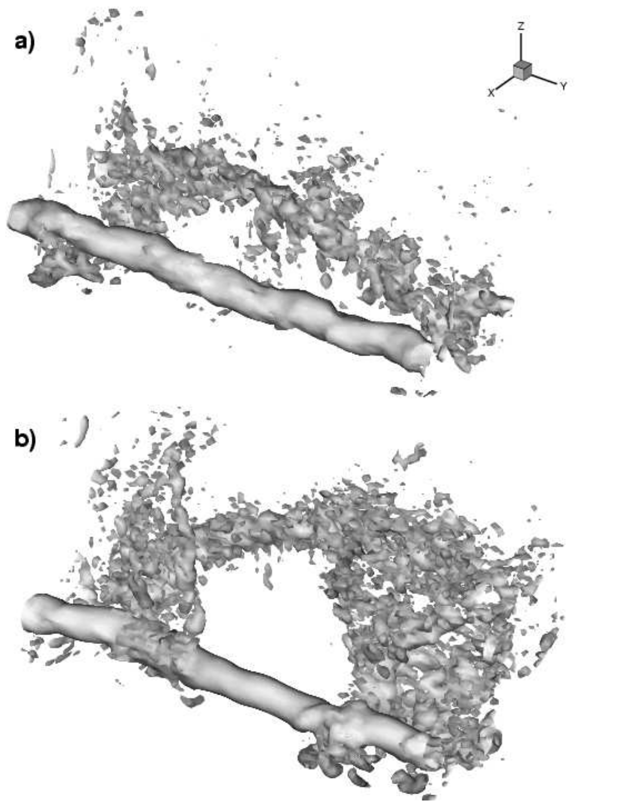

Fig. 6 Cases T0 (a) and T2 (b) at $t^* = 17.4$: Isosurfaces of $\lambda_2^* = -26.5$.

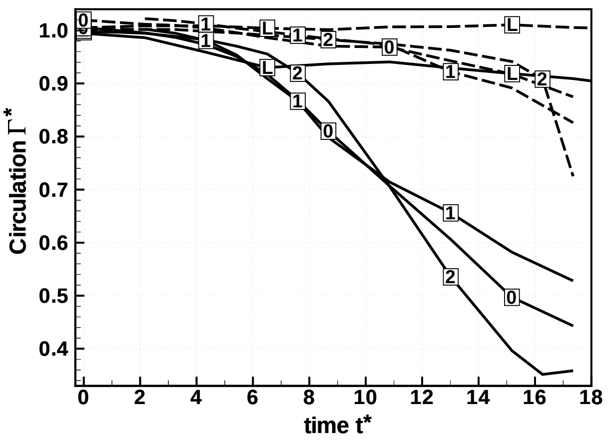

Fig. 7 Time series of circulation obtained at $r = 3r_c$ and averaged over y^*.

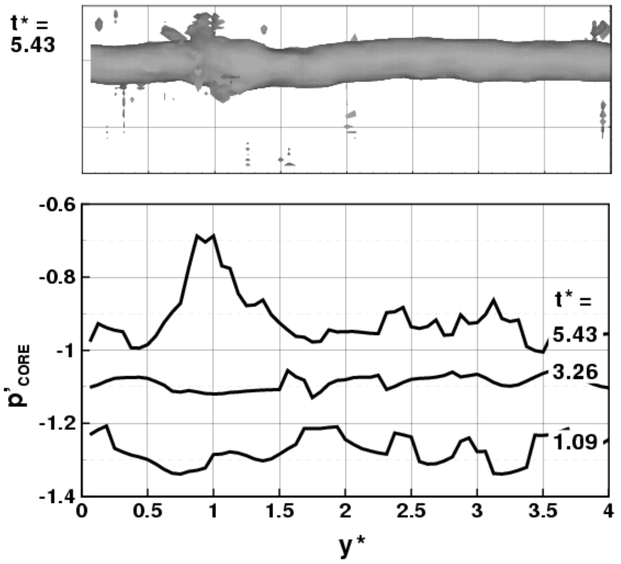

Fig. 8 Dynamic pressure deviation p'_{core} at the center of the upstream vortex vs. axial coordinate. The values are an average over 3^3 cells surrounding the local minimum of λ_2.

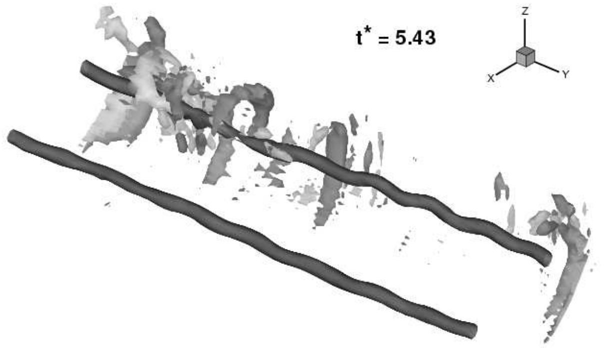

Fig. 9 Azimuthal structures and short–wave perturbations in case T0. Isosurfaces of azimuthal vorticity $\omega^*_\theta = -6.9$ (dark) and +6.9 (light) and of $\lambda^*_2 = -77.6$ with respect to upwind vortex location.

0.53 Γ_0 for T2, T0, T1, respectively. The Γ^* values of the downstream vortices of the turbulent cases decay slightly until $t^* = 11$ (for T0, T1) and 15 (for T2) and stronger afterwards. It is remarkable that the circulations of both upstream and downstream vortices of case T2 decay at higher rates in certain phases than their more turbulent counterparts T0 and T1. This bewildering result will be discussed in the next section. Changes in numerical resolution (T0 versus T1) only manifest slightly at times later than $t^* = 11$.

Discussion

Vortex core bursting has been extensively investigated in the framework of swirling jet streams.? The vortex core bursts when the axial flow stagnates and then reverses which is typically driven by an adverse pressure gradient due to the jet spreading. The stagnation of axial flow causes the jet to spread further which again increases the adverse pressure gradient. The stagnation of axial velocity demands the radial outflow of fluid from the core region which deforms the vortex filaments towards greater radial distances. The positive feedback in swirling jet flows amplifies the redistribution of axial to radial and azimuthal vorticity and the vortex bursts.

In our case, the two anti-parallel vortex tubes induce swirl but no flow along the vortex axes and no mean pressure gradient is superimposed. Nevertheless, Figure 8 reveals that the dynamic pressure deviation p'_{core} at the center of the (upstream) vortex slightly fluctuates around average values at early times ($t^* = 1.09$ and 3.26) until it suddenly increases significantly at $t^* = 5.43$ just before and decreases again just after $y^* = 1$. (The average increases monotonically in time because the core grows by diffusion.) Such a pressure "wall" may result when a convergent axial flow is induced by azimuthal structures surrounding the upstream vortex. In fact, Figure 9 shows that at $t^* = 5.4$ the upstream vortex has created contiguous azimuthal vorticity structures at the upwind side of the vortex by stretching the surrounding turbulent eddies.? These structures are not visible at $t^* = 1$ and 3.3. The two prominent structures of ω^*_θ to the left and right of the core burst (at $y^* = 1$) are indeed oriented such that they induce a convergent flow along the vortex axis.

The flow evolution in case T2 sustains our interpretation: Here we observe that Γ^* starts to decay rapidly at $t^* \approx 7$. This coincides with the time 7.6 when the corresponding azimuthal vorticity structures are developed and the core of the upstream vortex starts to burst (not shown). The event occurs later in case T2 than in case T0 since it takes longer to stretch the weaker eddies to a strength that is sufficient to induce a noticable flow along the vortex axis. The fact that Figure 7 depicts lower Γ^* values for T2 than for T0 at late times ($t^* = 17.4$) can be attributed to the strong curvature and the large diffusion of the upwind vortex, see Figure 6; we recall that Γ^* only takes into account the axial component of the vorticity vector within a radius of $3r_c$. The same argument holds for the abrupt decay of the downwind vortex at that time because we observe that fractions of the destroyed upwind vortex touch the almost intact downwind mate at several locations. The quickly diffusing core of the upstream vortex also may explain the apparently stronger decay of Γ^* between $t^* = 9$ and 16 of case T2 compared to cases T0 and T1.

Figure 10 compares core locations of the upwind and downwind vortices of cases L and T0. We see that the upwind vortex descends faster in turbulent environments whereas its downstream mate descends at the same speed as in a laminar jet. The less coherent

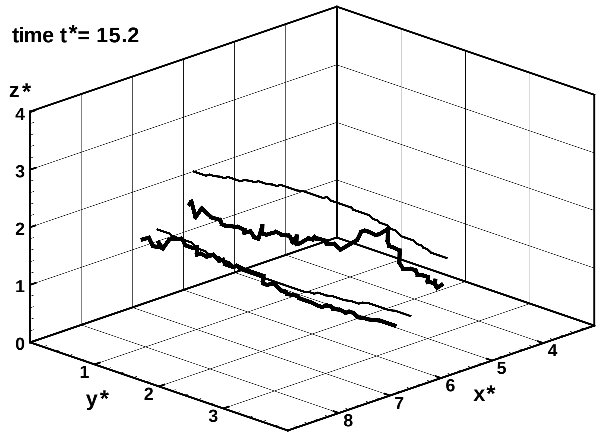

Fig. 10 Vortex trajectories for cases L (thin curves) and T0 (thick curves).

secondary vorticity of the upper shear layer of the turbulent jet induces less upward motion on the upwind vortex than in the laminar case such that the influence of the downwind partner is relatively stronger and the upwind vortex descends quicker and stays closer to its partner. On the other hand, owing to the closer spacing between the two vortices (roughly 30–50% of the spacing in the laminar case) also the upwind vortex can induce significant downwash on its downwind mate although its circulation has dropped to slightly more than 50% of Γ_0. Hence, the similar reductions of b and Γ_{up} cancel each other such that the induced flow of the upwind vortex on the downwind vortex is approximately the same for cases L and T0.

Conclusion

Three-dimensional direct numerical simulations have been carried out in order to investigate the behaviour of a counter-rotating vortex pair subjected to a laminar and two different turbulent low-level jets. For the laminar case, the vortex pair remains stable although sinusoidal deformations are prominent and the vortices later interact with the ground. On the other hand, when the jet is turbulent, we observe a mutually independent dissolution of each vortex. The upstream vortex with vorticity opposing the vorticity of the upper part of the jet erodes when penetrating into the jet, whereas the downstream vortex remains unaffected until it interacts with the part of the jet below the wind maximum.

Variation in jet turbulence intensity (cases T0 and T2) does not change the quality of erosion but modifies the decay in details which are not fully understood yet. Our variation of the numerical resolution (case T1) did not alter the results significantly. However, larger resolutions are required for a more detailed analysis of processes in the vortex core.

We postulate that the mutually independent erosion of the vortices is initiated by events similar to vortex–core bursting. Those events are triggered by the convergent flow along the vortex axis which, in turn, is induced by azimuthal structures. Risso *et al*? argue that those azimuthal structures around the main vortices, which were formed by stretching environmental turbulent eddies in the vicinity of the vortices, are responsible for the vortex deformation which initiates the long wave (Crow) instability. Here, we see that such ring–like structures also may be a possible candidate for the origin of vortex core bursts. The ring fragments may even propagate along the vortices to a certain extend (see plot on title page) which may explain the observed motion of the breakdown event along the axis.

Future work will concentrate on the differences between evolutions of cases T0 and T2 (impact of turbulence intensity) and the role of azimuthal and radial vorticity structures on the decay process.